An experimental study of boiling two-phase flow in a vertical rod bundle with a spacer grid-Part 2: Effects of vane angle

Tas-Köhler, S.; Boden, S.; Franz, R.; Liao, Y.; Hampel, U.;

Originally published:

July 2023

Experimental Thermal and Fluid Science 145(2023), 110903

DOI: https://doi.org/10.1016/j.expthermflusci.2023.111000

Perma-Link to Publication Repository of HZDR:

https://www.hzdr.de/publications/Publ-36690

An experimental study of boiling two-phase flow in a vertical rod bundle with a spacer grid-Part 2: Effects of vane angle

Sibel Taş [a]*, Stephan Boden [a], Ronald Franz [a], Yixiang Liao [a], Uwe Hampel [a,b]

[a] Helmholtz-Zentrum Dresden-Rossendorf, Institute of Fluid Dynamics, Bautzner Landstr. 400, 01328 Dresden, Germany

[b] Technische Universität Dresden, Chair of Imaging Techniques in Energy and Process Engineering, 01062 Dresden, Germany

* Corresponding author (E-mail: s.tas@hzdr.de)

Abstract

We performed boiling flow experiments and measured the void fraction in a 3 x 3 rod bundle including a spacer grid with split type vanes using X-ray computed tomography, which provides high-resolution time-averaged void data without disturbing the flow. We studied the effects of mixing vanes with different vane angles, namely, 20°, 29° and 40°, for a mass flux between 535 and 1950 kg/m^2 s and the central rod being heated giving a heat flux of 85.7 kW/m^2. The experiments were conducted using octafluorocyclobutane (RC318) as the working fluid. The presence of vanes leads to an increase of the cross-sectional averaged void fraction up to an axial position of $Z \approx 0.8D_h$. After that, the void fraction decreases until $3D_h < Z < 4D_h$ due to the induced swirl flow, before it increases again. It was further found that the vanes cause a high local void fraction near the spacer, which increases the possibility of DNB occurrence. From this study, it can be concluded that a vane angle of 29 ° is optimal for two-phase flow, which is consistent with the findings in the literature for single-phase flow.

Keywords: Fuel element, spacer, vane angle, X-ray computed tomography, void fraction

Nomenclature

Latin symbols		**Greek**	
D_h	Hydraulic diameter (mm)	α	Phase fraction (-)
G	Mass flux (kg/m^2·s)	μ	X-ray attenuation coefficient (m^{-1})
q	Heat flux (kW/m^2)	ρ	Density (kg/m^3)
r	Radius (mm)	**Subscripts**	
P	Pressure (Pa)	L	Liquid
u	Velocity (m/s)	G	Gas
$w(i,j,Z)$	Weight function	TP	Two-phase
X	Lateral position (mm)		
Y	Lateral position (mm)		
Z	Axial position (mm)		

Acronyms

CT: Computed Tomography
CFD: Computational Fluid Dynamics
CHF: Critical Heat Flux
DNB: Departure from Nucleate Boiling
DNBR: Departure from Nucleate Boiling Ratio
LDA: Laser Doppler Anemometry
LDV: Laser Doppler Velocimetry

MTF: Modulation Transfer Function
PWR: Pressurized Water Reactor

1. Introduction

In water-cooled reactors, forced water flow in the reactor core takes up the fission heat for electricity production. When the heat is not efficiently removed from the fuel rod surfaces, local heat build-up can lead to damage of the fuel assemblies. In pressurized water reactors (PWRs) single-phase flow is prevailing, but a certain amount of sub-cooled boiling flow is also allowed during normal operation. A high boiling rate can occur in PWRs during transients or accident conditions (Colombo and Fairweather (2016)). Accumulation of steam may then lead to departure from nucleate boiling (DNB), which is characterized by the formation of a vapor film in some locations on the fuel rods, which reduces heat transfer to the coolant and increases rod wall temperature above critical values. This phenomenon is called critical heat flux (CHF). In order to increase the efficiency of heat transfer and thus reduce the risk of CHF, spacer grids with mixing vanes are frequently used in fuel assemblies. Spacer grids themselves have the function to maintain a constant distance between the rods and to suppress flow-induced vibrations that may lead to fretting corrosion (Pickman (1972)). Mixing vanes on the spacer grids promote enthalpy exchange in the fuel element by generating either a swirling or a cross-channel flow. Therefore, the design and optimization of the mixing vanes are very important to increase the reactor safety.

Most studies on mixing vanes in the literature have been performed for single-phase flows (Bhattacharjee et al. (2017); Kim and Seo (2005); Moon et al. (2014); Wang et al. (2019); Wang et al. (2020); Wei et al. (2021)). The vane type and vane angle are the two most significant design parameters of a spacer grid, as they determine the effective mixing length and thus the distance between the two spacers. In (2001) found that split vanes and twisted vanes provide a higher mixing rate for both swirl and cross-flow than side-supported vanes and swirl vanes. Han et al. (2009) found that the mixing effect of the spacer grid with tandem arrangement vanes (vanes arranged in series) is stronger than that of the spacer grid with split vanes. Chang et al. (2008) and Chang et al. (2014) found that a split vane produces higher turbulence intensity and provides better mixing efficiency between sub-channels than a swirl vane. Considering the vane angle, a larger vane angle results in a higher mixing rate (Shen et al. (1991)). However, as the vane angle increases, the pressure drop in the rod bundle also increases. In terms of design, a high pressure drop is undesirable as it affects pump power, i.e. operating costs. Therefore, a vane angle of about 29° was found to be optimal in terms of heat transfer and pressure drop (Cheng et al. (2017); Shen et al. (1991); Tas-Koehler et al. (2020); Wu et al. (2017)). The mixing effect, which depends on the vane type and angle, is dominant up to a certain length through the rod bundle. Cui and Kim (2003) reported that the mixing effect of the vanes decreases from the vane tip $L = 0$ to $L \approx 4D_h$ (D_h is the hydraulic diameter) and Tas-Koehler et al. (2020) found that it is up to $L \approx 7D_h$ for a vane angle of 29°. The mixing effect is important because it directly affects heat transfer. Holloway et al. (2008) showed that for split-type vanes, the heat transfer coefficient initially increases in the range $0 < L < 1.5D_h$ and then decreases exponentially with the streamwise distance. Byun et al. (2018) found that for split vanes, the improvement in heat transfer occurs in the range $0 < L < 10D_h$. In et al. (2015) found that the heat transfer coefficient downstream of the twist vane ($L > 0$) is about 30% higher than in the region upstream of the vanes ($L < 0$).

With regard to reactor safety in PWRs, studies have shown on the one hand that mixing vanes increase CHF (Decrecy (1994); Shin and Chang (2005)). Li et al. (2021) performed a sub-channel analysis in a rod bundle and found that compared to a spacer grid without mixing vanes, the grid with mixing vanes increases the departure from nucleate boiling ratio (DNBR) of fuel rod surface and in the axial direction by about 5%–14%, suppresses the boiling crisis. On the other hand, it has been reported that vanes can increase the localized void fraction on the heated rod surface, which can lead to a boiling crisis, i.e. reaching CHF (Cong et al. (2018)).

In addition, the behaviour of the two-phase flow around the spacer in the rod bundle is particularly important because a boiling crisis often occurs near or in the spacer (Takenaka et al. (1996)).

The effect of mixing vanes in two-phase flows has rarely been investigated. Ren et al. (2018) conducted air-water two-phase flow experiments in a 5 x 5 rod bundle with mixing vane spacer grids (MVSGs) and measured void fraction with a four-sensor conductivity probe. They showed that the skewed peaks of the void fraction are connected with the direction of mixing vanes and a larger value of the area-averaged void fraction is induced downstream of MVSG. They recommended further investigations for a detailed understanding. For an optimum vane angle, Shin and Chang (2005) investigated the effect of the vane angle and position of the mixing vanes on the vortex flow in a 2 x 2 rod bundle. They found that when the vane angle is relatively small, the magnitude of the vortex flow is smaller because the rotational force by the mixing vane is weak; however, when the angle is too large, the mixing vane plays the role of a flow obstacle under the DNB condition. Then the flow deflected by the individual vanes cannot establish a proper swirling flow. Therefore, it was reported that the optimum vane angle is 30°, which provides maximum mixing. Yang et al. (2021) numerically investigated five different vane angles, i.e. 18°, 24°, 30°, 36° and 42°, in a 3 x 3 rod bundle and analysed the influence of the vane angles on the flow and heat transfer of coolant. They reported that as the vane angle continued to increase from 30°, the relative increase of the cross-flow factor declined, which shows that the 30° is the critical vane angle. A similar conclusion was also found in the analysis of near-wall void fraction, wall superheat and liquid convection heat flux. The details of the aforementioned studies are given in Table 1. Although the general agreement on the optimum angle for two-phase flow seems to be around 30°, as for single-phase flow, this optimized angle should be supported by further investigations under different heat and mass flux conditions (Mimouni et al. (2011)).

Table 1: Summary of studies on mixing vanes taken from the literature.

Researchers	**Geometry**	**Vane type and angle**	**Single-phase/ Two-phase**
Experimental			
Shen et al. (1991)	4 x 4 rod bundle	mixing blades (0°, 20°, 25°, 30°, 35°)	single-phase (water)
Shin and Chang (2005)	2 x 2 rod bundle	mixing vanes produced by KAERI (20°, 30°, and 40°)	two-phase (R-134a)
Chang et al. (2008)	5 x 5 rod bundle	split vane (30°), swirl vane (35°)	single-phase (water)
Holloway et al. (2008)	5 x 5 rod bundle	standard grid, split vane (30°) disc vane	single phase (air)
Han et al. (2009)	6 x 6 rod bundle	tandem arrangement vanes (30°)	single-phase (water)
Chang et al. (2014)	5 x 5 rod bundle	split vane, swirl vane	single-phase (water)
Moon et al. (2014)	6 x 6 rod bundle	split vane	single phase (steam)
In et al. (2015)	3 x 3 rod bundle	twisted vane (35°)	single-phase (water)

Byun et al. (2018)	6 x 6 rod bundle	split type, large scale vortex flow type (30°)	single-phase (water)
Ren et al. (2018)	5 x 5 rod bundle	spacers with vanes	two-phase (air-water)
CFD			
In (2001)	single sub-channel	split vane (30°), side-supported vane, swirl vane, twisted vane (35°)	single-phase (water)
Cui and Kim (2003)	single sub-channel	NJ type vane (25°), split vane (25°)	single-phase
Kim and Seo (2005)	two sub-channel	split vane (25°), split vane with cutout (29°)	single phase
Cheng et al. (2017)	5 x 5 rod bundle	split vanes (25°, 31°, 37° and 43°)	single phase
Wu et al. (2017)	four sub-channel	rectangular longitudinal vortex generators (30°, 45°, 60°)	single phase
Bhattacharjee et al. (2017)	flow around a rod	square spacer grid, circular spacer grid, mixing vane (30°)	single phase
Wang et al. (2019)	5 x 5 rod bundle	spacer with vanes (20°, 25°, 30° and 35°)	single phase
Tas-Koehler et al. (2020)	single sub-channel	split vanes (20°, 25°, 29°, 32° and 40°)	single phase
Wang et al. (2020)	5 x 5 rod bundle	spacer with split vanes	single phase
Yang et al. (2021)	3 x 3 rod bundle	spacer with vanes (18°, 24°, 30°, 36° and 42°)	two-phase (water-steam)
Wei et al. (2021)	5 x 5 rod bundle	spacer with split vanes	single phase (water)

The literature review shows that many studies were conducted on the effects of mixing vanes on single-phase flows, while studies on two-phase flows are less common. In addition, the existing literature on the effects of vane angle in boiling two-phase flows is limited and experimental analysis of the effects of vane angle under different flow conditions, such as mass flux, have not yet been performed. Thus, the effects of mixing vanes on two-phase flow are not yet well known in detail. Moreover, the location of DNB occurrence is closely related to the design of the mixing vanes. Therefore, the optimization of the vane angle is a primary concern for fuel element design and safety assessment.

In this context, the present study aims to address the effects of vane angle on the void fraction in boiling two-phase flow conditions for different mass flux conditions. For this purpose, we performed boiling flow experiments in a 3 x 3 rod bundle including a spacer grid with split type vanes. We measured the void fraction using X-ray computed tomography (CT). We analyzed the effects of different vane angles, i.e. 20°, 29° and 40°, on the distribution of the void fraction. In addition, a spacer without vanes was also compared to a spacer with vanes.

2. Experimental setup

The experiments were performed with RC318 by applying fluid scaling with reference to pressurized water reactor conditions. Table 2 shows the experimental conditions. The operating pressure of the system is around $5 \cdot 10^5$ Pa. The inlet temperature of the working fluid is around 35°C. Four different mass fluxes were applied in the experiments. As shown in Figure 1, the rods have an outer dimeter of 10 mm and they are vertically arranged in the test section. The pitch between the rods is 12.8 mm. Test section is partially heated. The length of the heating zone is 330 mm. All the rods are heated, but the heating power ratio from center rod to outer rods is 64:1.

Therefore, boiling takes place only around the center rod. The electrical heating current is controlled and the circuit contains a fast switch-off, triggered by a fiber optical temperature measurement system (ODiSI B from LUNA Inc., Roanoke, VA, USA). A spacer grid equipped with split type vanes is inserted in the rod bundle. The upper edge of the spacer is set as the reference height (i.e. $Z = 0$). The design of the split vanes is shown in Figure 2. More details about the experimental setup can be found in the first part Taş et al. (2023).

Table 2: Experimental conditions.

Parameter	**Values**
Mass flux (kg/m^2 s)	535 (G_1), 1070 (G_2), 1605 (G_3), 1950 (G_4)
Pressure (pascal)	~$5{\cdot}10^5$
Heat flux applied to the center rod (kW/m^2)	85.7
Subcooling temperature (K)	~10
Thermal power profile	Uniform
Vane angle (°)	20, 29, 40

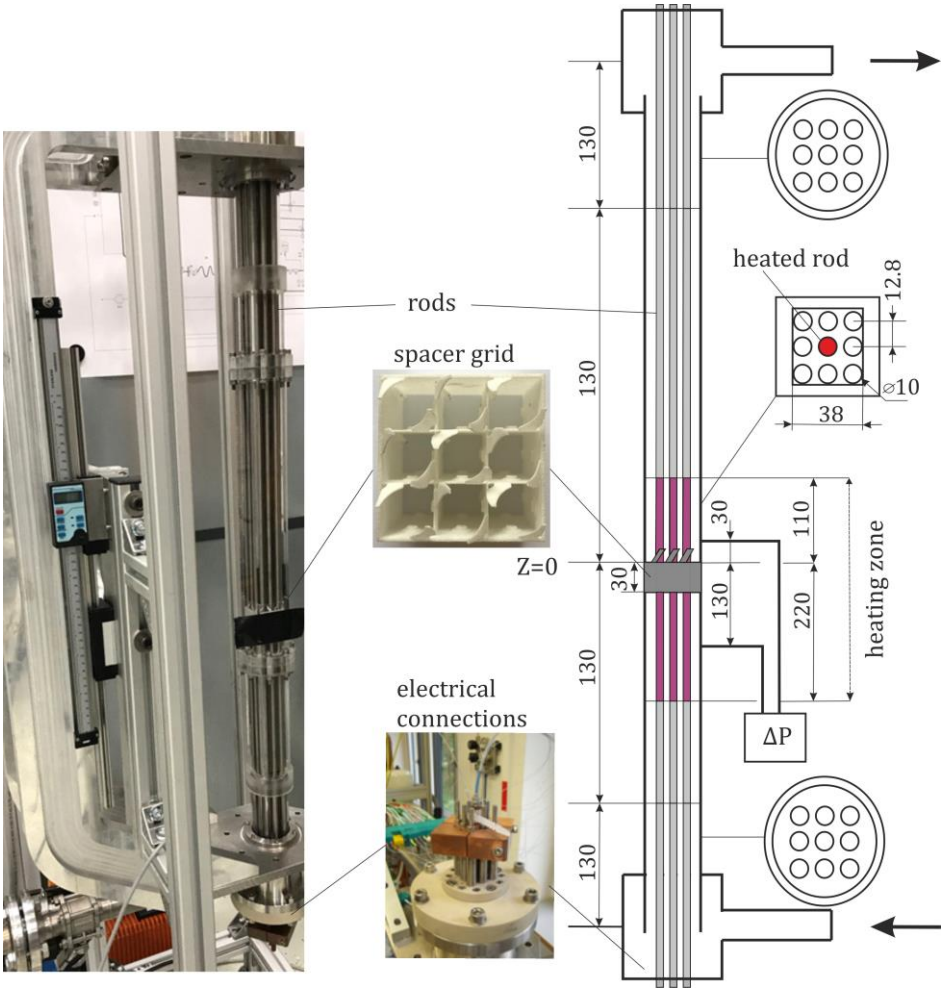

Figure 1: Photo (left) and schematic (right) of test setup (dimensions are in mm) (Taş et al. (2023)).

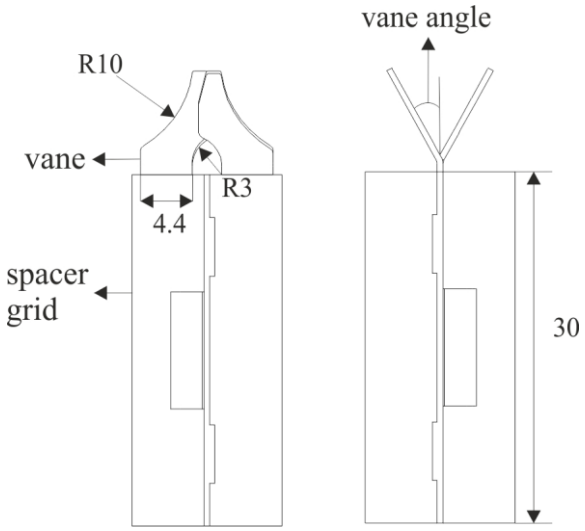

Figure 2: Schematic of the spacer grid equipped with two split vanes: front view (left) and side view (right) (dimensions are in mm).

A proprietary microfocus X-ray CT system, as shown in Figure 3, was used to measure three-dimensional (3D) void fraction distribution inside the bundle. It comprises a commercial microfocus X-ray tube (XrayWORX XWT-190-TC) and a two-dimensional flat-panel X-ray image detector (PerkinElmer XRD 0822 AP3 IND; 205×205 mm² total active area covered by 1024×1024 pixels). The X-ray tube and detector are attached to a motorized rotary stage (Aerotech AGR150) with the vertical rod bundle extending through the hollow shaft of the rotary stage. For a single scan the tube-detector assembly is driven along a circular orbit around the test section over an angular range of 360° at a speed of 0.3°/s, resulting in a duration of a single scan of twenty minutes. The distances between the rotational axis and the X-ray tube and detector are chosen so that the size of the scanned volume is 70 mm in the axial direction. To cover an axial range of 130 mm along the rod bundle axis two consecutive scans are required for each experimental configuration, whereby the whole test section is lowered by an axial distance of 60 mm for the second scan.

The average spatial resolution of the microfocus X-ray tomography setup was determined by calculating the modulation transfer function (MTF) of the raw reconstructed image data at the edges of the outer channel walls. The spatial frequency at which the MTF falls below 0.5 was measured to be 2.1 linepairs per millimeter (lp/mm) corresponding to a spatial resolution of approximately 240 μm. More details about the X-ray CT system and the uncertainty of the measurement system can be found in Taş et al. (2023).

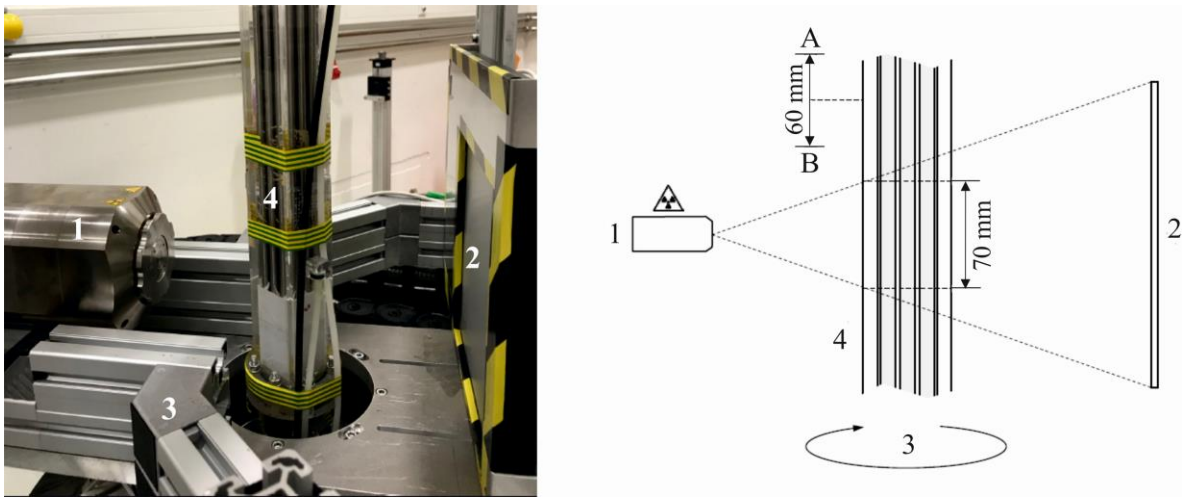

Figure 3: Photo (left) and schematic (right) of the high-resolution microfocus X-ray CT setup: 1 – X-ray tube, 2 – flat-panel X-ray image detector, 3 – rotating gantry, 4 – vertical rod bundle, A – 1st measurement position, B – 2nd measurement position (Taş et al. (2023)).

The 3D spatial distribution of the time-averaged effective X-ray attenuation coefficient $\mu(X,Y,Z)$ of the test section and the fluids flowing therein is reconstructed from the X-ray projection images using the Feldkamp-Davis-Kress algorithm (Feldkamp et al. (1984)). In the following equations, the coordinates (X,Y,Z) of the spatial distributions have been omitted for convenience.

To compute the local void fraction in the volume between the rods from the measured X-ray attenuation the well-established two-point calibration is utilized,

$$\alpha_G = 1 - \frac{\mu_{TP} - \mu_G}{\mu_L - \mu_G} = \frac{\mu_L - \mu_{TP}}{\mu_L - \mu_G} \tag{1}$$

with μ_G, μ_L and μ_{TP} being the time-averaged local effective X-ray attenuation of the vapor, the liquid and the two-phase mixture, respectively. Thus, additional scans of μ_{Empty} and μ_{Full} for the completely empty and liquid-filled test section are required. These reference scans are conducted with the test section being at room temperature. Therefore, Equation 1 is rewritten to account for the differences between the cold liquid density (ρ_{L_cold}) and hot liquid density (ρ_{L_hot}):

$$\alpha_G = \frac{\left(\mu_{Full_{cold}} - \mu_{Empty_{cold}}\right) - \left(\mu_{Boiling} - \mu_{Empty_{hot}}\right)\frac{\rho_{L_{cold}}}{\rho_{L_{hot}}}}{\mu_{Full_{cold}} - \mu_{Empty_{cold}}}. \tag{2}$$

With $\mu_{Empty\_cold} \approx \mu_{Empty\_hot}\frac{\rho_{L\_cold}}{\rho_{L\_hot}}$, Equation 2 simplifies to

$$\alpha_G \approx \frac{\mu_{Full} - \mu_{Boiling}\frac{\rho_{L_{cold}}}{\rho_{L_{hot}}}}{\mu_{Full} - \mu_{Empty}}, \tag{3}$$

requiring only one single empty reference scan.

Due to the strong streaking image artefacts in the difference image $\mu_{\text{Full}} - \mu_{\text{Empty}}$, the attenuation difference $\mu_{\text{Full}} - \mu_{\text{Empty}}$ is replaced by a constant μ_{Ref}. It is obtained as follows: the difference image $\mu_{\text{Full}} - \mu_{\text{Empty}}$ is forward projected (integrated) in the frontal and sagittal directions and the obtained integral attenuation profiles are divided by the profiles of geometrically known path-lengths through the liquid, and the resulting attenuation coefficients are averaged. Finally, the local void fraction is calculated using

$$\alpha_G \approx \frac{\mu_{Full} - \mu_{Boiling} \dfrac{\rho_{L_{cold}}}{\rho_{L_{hot}}}}{\mu_{Ref}}. \tag{4}$$

For details on the post process and data analysis, the interested reader is referred to Taş et al. (2023).

3. Results

In a typical vane design, the vane angle is generally between 20° and 30° (Tiftikçi et al. (2013)). Based on this, we measured the void fraction for four different mass fluxes and three different vane angles, i.e. 20°, 29° and 40° (Table 1), for a heat flux of 85.7 kW/m^2. The mixing vanes are in the range $0 < Z < 0.77D_h$. We also measured the void fraction of spacer grid without mixing vanes for the comparison. Figure 4 shows the cross-sectional averaged void fraction in the axial direction, which is calculated by

$$\overline{\alpha_{\text{G}}}(Z) = \frac{1}{\sum_{ij} w(i,j,Z)} \sum_{ij} w(i,j,Z) a_{\text{G}}(i,j,Z) \tag{5}$$

with (i,j) being the corresponding image coordinates in pixels. The weight function $w(i,j,Z)$ defines a pixel mask with $w(i,j,Z) = 1$ for pixels in the fluid domain and $w(i,j,Z) = 0$ for all other pixels.

The horizontal axis in the figure is given as Z/D$_{\text{h}}$, where $D_h = 10.86$ mm is the hydraulic diameter of the rod bundle.

As a side-note: in the region of the titanium clamps holding the fiber optic temperature sensor, the void fraction values have a high uncertainty due to rather high radiation attenuation and associated artefacts in the reconstructed data, as shown in Figure 4a. These artefacts in turn lead to local errors in the void fraction data calculated from the images, and so that local void fraction data in the immediate vicinity of the titanium clamps have to be considered as unreliable. For instance, the local fluctuations in the void fraction profile in Figure 4b in the gray-shaded areas are not physical jumps in void fraction, but are only measurement uncertainties due to the effects described above. More details about the uncertainties can be found in Taş et al. (2023).

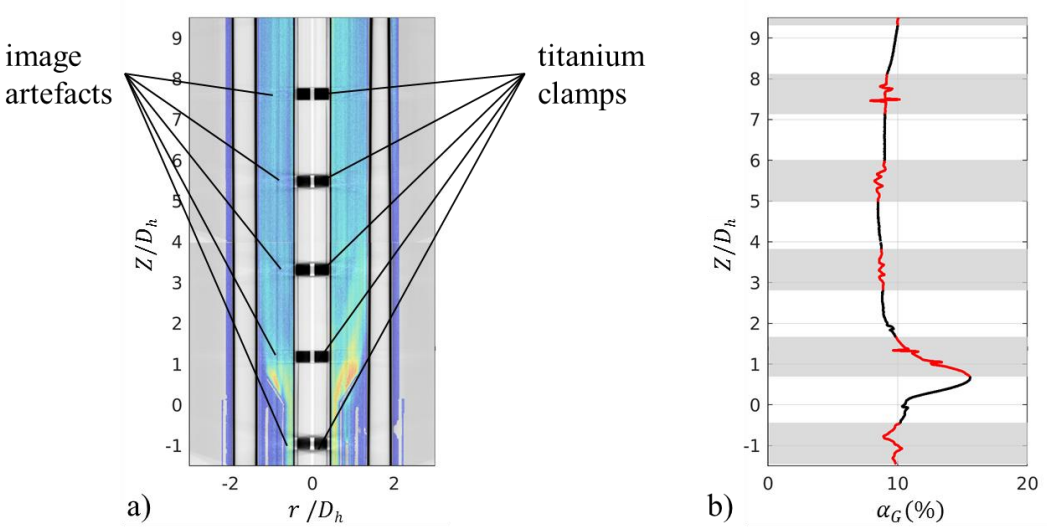

Figure 4: High density titanium clamps causing measurement artefacts. a) Arbitrary raw tomographic slice image of the test section (grayscale) and corresponding void fraction distribution (colors). b) Corresponding integral void fraction profile with remarkable erroneous fluctuations (gray background) (Taş et al. (2023)).

The averaged void fractions at different vane angles, i.e. 20°, 29° and 40°, in axial direction for different mass fluxes are shown in Figure 5. The effect of vanes on the averaged void fraction is shown to be dependent on both the mass flux and the vane angle. For the mass flux G_1, all the vane angles cause more or less the same averaged void fraction in the range $1D_h < Z < 3D_h$. After $Z = 3D_h$, the vane angle 40° causes a higher void fraction downstream compared to the other two vane angles, whereas the vane angles 20° and 29° show a similar behaviour. "No vane" case causes the lowest void fraction in the range $4D_h < Z < 7.5D_h$. For the mass flux G_2, the "no vane" case has a higher void fraction than the cases with vanes after $Z = 1D_h$ and the vane angle 29° has the lowest void fraction thereafter. Vane angles 20° and 40° result in a similar void fraction in the range $1.5D_h < Z < 4D_h$, while vane angle 20° results in a lower void fraction after $Z = 4D_h$. In addition, after $Z = 7D_h$, the difference between vane angles 20° and 29° becomes very small. For the mass flux G_3, the vane angles 29° and 40° have similar void fractions in the range $1.5D_h < Z < 3.5D_h$. After $Z = 3.5D_h$, the vane angle 29° has the lowest void fraction. For the mass flux G_4, the performances of all vane angles, especially vane angles 29° and 40°, are similar.

One of the interesting results is that the vane angle 40° causes a relatively high void fraction after the flow passes the vanes compared to the other vane angles, although all the tests show a peak in the vane region. It indicates that in this region the heat transfer from the heated rod is intensified by the vanes, enhancing the production of gas. In addition, this angle can cause flow separation, resulting in low pressure areas, as reported in the study by Tas-Koehler et al. (2020). In this case, the bubbles may accumulate in the low pressure areas, resulting in high local void fraction. The increase in maxima of the vane angle 40° compared to the vane angle 29° appears in G_2 with a value of approximately 43%. Note that for the spacer grid without vanes, the void fraction also increases from $Z = 0$, which is probably due to the pressure and velocity changes within the spacer.

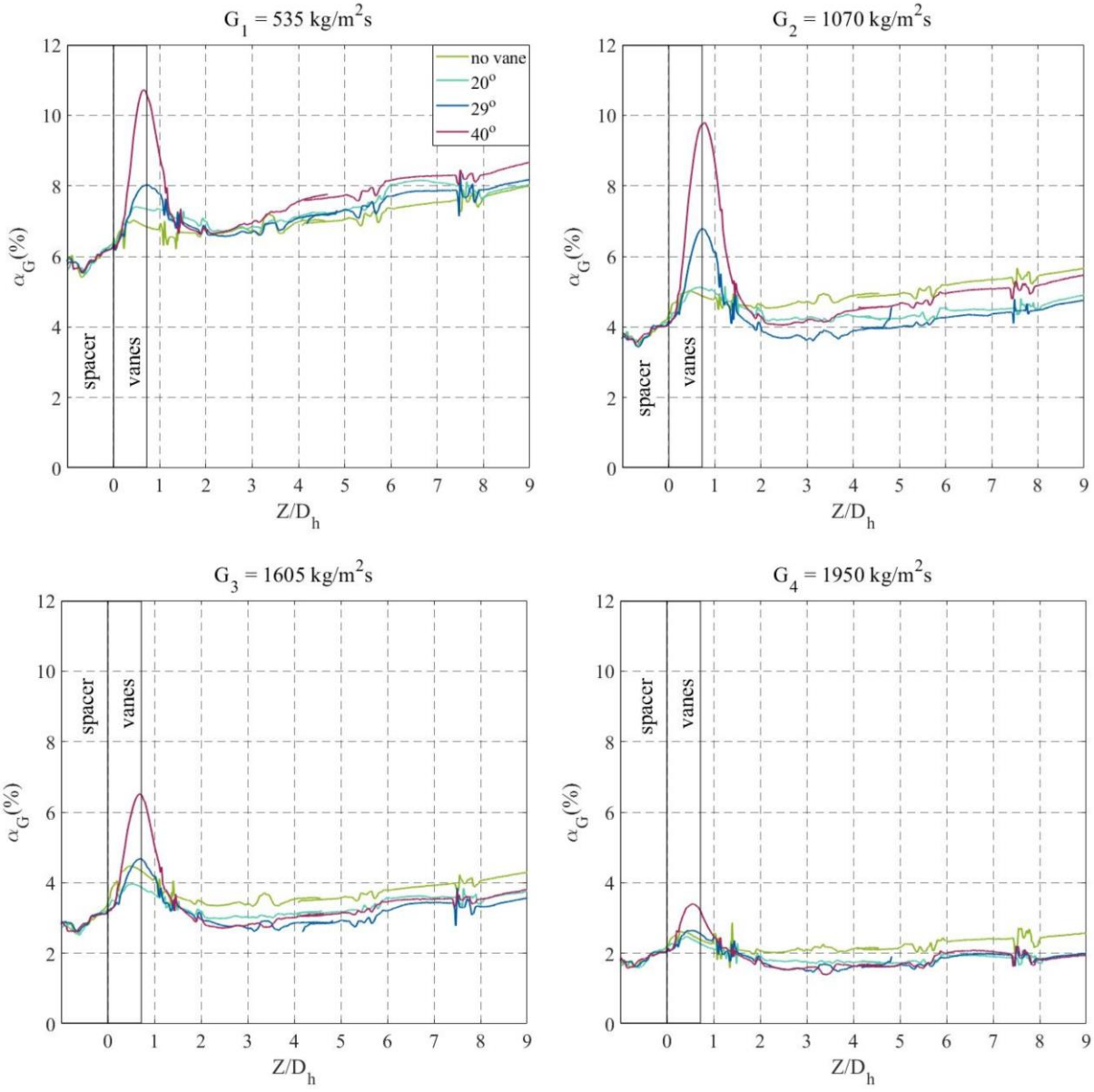

Figure 5: Cross-sectional averaged void fraction in the axial direction for three vane angles at different mass fluxes. The "no vane" case is also included for the comparison.

The effect of vanes on the flow field mainly results from two aspects, namely, increasing the velocity and changing the flow direction. The former tends to enhance the heat transfer and increase the vaporization, while the latter helps to sweep the gas away from the heated surface and reduce the averaged void fraction in the surrounding sub-channels. In the vane region, the enhancement of heat transfer is dominant. Therefore, the void fraction increases especially for large vane angles. Downstream of the vane, the mixing effect becomes dominant compared to the heat transfer enhancement. From Figure 5 one can see that at low mass fluxes, e.g. G_1, the latter effect is still stronger than the former one, and as a result, the void fraction at all vane angles is higher than in the "no vane" case. With the increase of mass flux, the mixing effect becomes dominate compared to the heat transfer enhancement, and consequently, the presence of vanes decreases the averaged void fraction around the heated rod.

In principle, the larger the vane angle the higher the heat transfer and the mixing effect, but downstream the vane with an angle of 29° has a better mixing effect compared to its heat transfer improvement, and therefore, the void fraction is the lowest. Nevertheless, at very high mass fluxes, e.g. G_4, the effect of the vane angle on the mixing becomes negligible.

Figure 6 shows the cross-sectional distributions of the void fraction for different vane angles for $G_1 = 535$ kg/m^2 s in different Z positions. For the "no vane" case, the void accumulates around the heated rod, which may lead to boiling crisis.

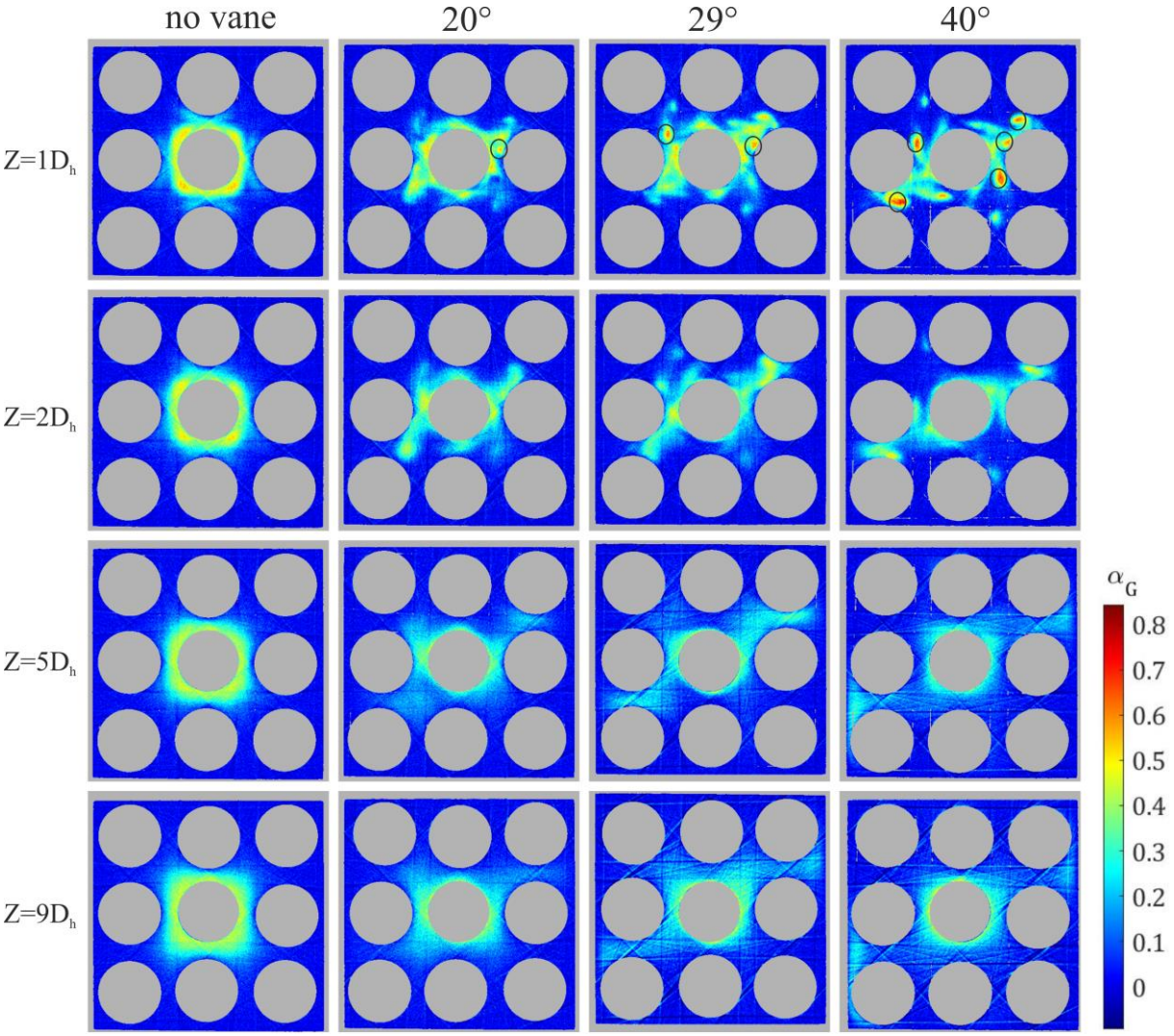

Figure 6: Cross-sectional void distribution for $G_1 = 535$ kg/m^2 s at different axial positions.

The gas generated at the central heated rod surface is distributed to the surrounding sub-channels. At $Z = 1D_h$, discrete areas with relatively high void fraction ($\alpha_G \approx 0.7$) occur due to the vanes, which are indicated with black circles in the figure. In agreement with Figure 5, as the vane angle increases, the amount of void fraction in these areas increases. At $Z = 2D_h$, void fraction in these areas decreases, and they shift further towards other neighboring sub-channels due to the mixing effect. Moreover, as the vane angle increases, these high void fraction areas reach different circumferential regions of the neighboring rods due to the swirl flow forming in the sub-channels. At $Z = 5D_h$, the areas with a relatively high void fraction disappear and the void continues to be distributed laterally across the cross-section. Note that from this distance, some bubbles reach the gap between the rod bundle and the channel wall. At $Z = 9D_h$, the amount of void around the center rod increases again due to vaporization. It can be seen that the vanes help to wash the void away from the heated surface and avoid the occurrence of DNB. However, during the process localized high void fraction spots are formed in the sub-channel region. This localized void fraction may shift to surrounding rod surfaces depending on the flow conditions, which may again promote DNB at these positions. More investigation is required to clarify this.

The spacer grid in the present study includes two dots and a rectangular plate to hold each rod in position. This is shown in Figure 7, which illustrates the four quadrants around the heated rod, $\theta = [0, \pi/2], [\pi/2\,, \pi], [\pi, 3\pi/2], [3\pi/2\,, 2\pi]$ and the arrangement of the vanes. The azimuthal distributions of the averaged void fraction in an annular region with a distance between 0.25 mm to 0.75 mm from the center rod surface at G_1 are shown in Figure 8. Due to mechanical vibrations during the boiling process and temperature-induced shifts in the position of the rods between reference and boiling measurements, the accuracy of the results at a distance of up to 0.25 mm away from the rod surfaces remains uncertain, and thus data from pixels at a distance of less than 0.25 mm were not considered in the analysis.

It is clear that in the "no vane" case, only the components within the spacer, i.e. $Z < 0$, have an effect on the void distribution around the rod, which is represented by the three blue points. In the downstream region, $Z > 0$, the distribution is rather uniform. For the cases with vanes, there are areas of relatively low void fraction in all four quadrants due to swirling flow. The arrangement of vanes is shown to have an effect on the void distribution, which is similar in the quadrants $\theta = [0, \pi/2]$ and $[\pi, 3\pi/2]$, while similar in $\theta = [\pi/2\,, \pi]$ and $[3\pi/2\,, 2\pi]$. For vane angle 20°, the lowest void fraction is present in the quadrants $\theta = [\pi/2\,, \pi]$ and $[3\pi/2\,, 2\pi]$. As the vane angle increases to 29°, these areas enlarge, i.e. the vane angle 29° results in a lower void fraction around the centre rod than the vane angle 20° in the above two quadrants. At angle 40°, the swirling flow caused by the vanes is obviously stronger than the flow caused by the other two angles, and the orientation of the low void fraction areas becomes more in line with the swirling direction directly downstream of the vane, i.e. $Z < 4D_h$. Another point is that while the effect of the vanes on the void fraction at angle 20° and 29° continues up to $Z \approx 10D_h$, at the vane angle 40° the effect of vane angle on void fraction continues up to $Z \approx 7D_h$.

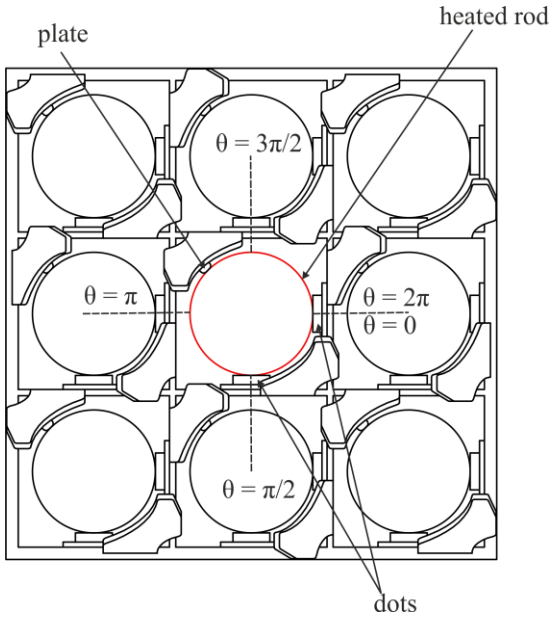

Figure 7: Schematic representation of the spacer demonstrating the azimuthal orientation of the center rod (θ = 0 − 2π) (Taş et al. (2023)).

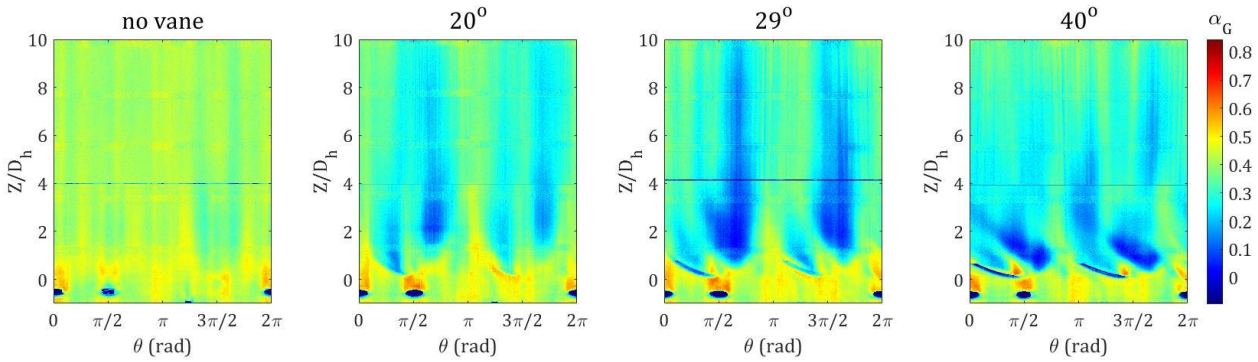

Figure 8: Azimuthal averaged void fraction in annular region 5.25 mm < r < 5.75 mm for $G_1 = 535$ kg/m^2 s along the central rod (for the orientation of θ see Figure 7).

Since this is an important parameter for the spacer grid design, the pressure drop between the inlet and outlet of the spacer (i.e. between $Z = -11.97D_h$ and $Z = 2.76D_h$) was also measured during the experiments and the results for the mass flux G_2 are given in Figure 9. From the no vane case to the vane angle 20°, the pressure drop increases by about 50%. From one vane angle to the other (i.e. from 20° to 29° and from 29° to 40°), the pressure drop changes by around 40%.

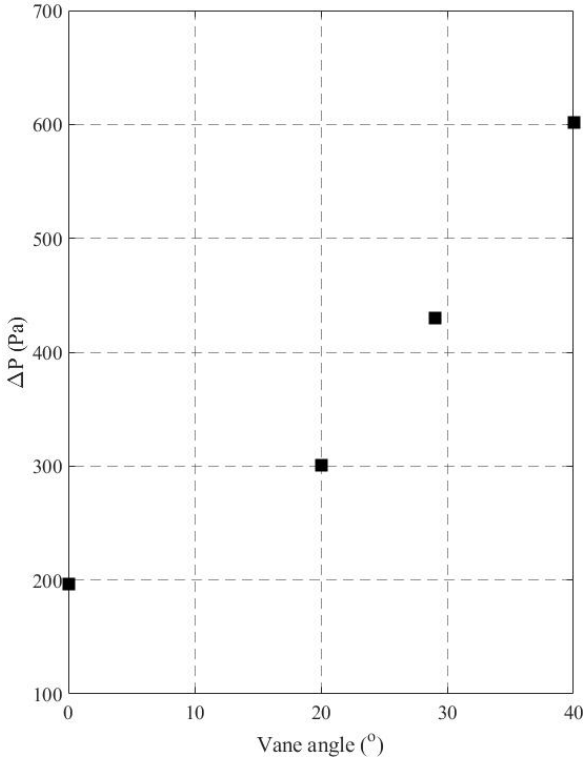

Figure 9: Pressure drop calculated as $\Delta P = \left|P_{Z=-11.97D_h} - P_{Z=2.76D_h}\right|$ against vane angle.

4. Conclusions

We performed boiling flow experiments using RC318 as the working fluid in a 3 x 3 rod bundle geometry with different vane angles under different mass flux conditions using the microfocus X-ray computed tomography technique, which enables to measure the time averaged and spatially highly resolved void fraction in the sub-channel without disturbing the flow.

The effects of the spacer are dependent on both the flow mass flux and the angle of the vanes. The averaged void fraction in the sub-channels surrounding the heated rod is affected by the enhancement in heat transfer and lateral mixing effect brought by the vanes. With the exception of the lowest mass flux, all vane angles result in a higher void fraction than in the "no vane case" downstream. The reason for this is that at the lowest mass flux, the effect of heat transfer is more dominant compared to the mixing effect. At the moderate mass fluxes, vane angle 29° provides the lowest void fraction compared to the other two angles. At the highest mass flux, all the angles cause a similar void fraction downstream. Another important result is that the vane leads to locally high void fraction when the flow passes over it, especially at a vane angle of 40°. In addition, areas of local high void fraction occur in the cross section just downstream of the vanes, and as the vane angle increases, the void fraction in these areas increases. Furthermore, the effect of the vanes on the void fraction continues for a larger distance along the flow direction at an angle of 20° and 29° than at a vane angle of 40°. Considering the pressure drop, it can be seen that as the vane angle increases, the pressure drop due to the spacer grid also increases. However, the pressure drop does not increase sharply at a vane angle of 40° compared to a vane angle of 29° as shown in previous studies for single-phase flow.

On the one hand, the vanes sweep off the void generated at the heated rod and reduce the cross-sectional averaged void fraction along the axial direction due to the swirl effects on the two-phase flow, which leads to a reduction in the possibility of occurrence of DNB downstream. On the other hand, they cause a locally high void fraction, especially for a large vane angle, which may affect the heat transfer of neighboring rods and increases the possibility of DNB occurrence. Considering all the mass fluxes, it can be concluded that a vane angle of 29 ° is optimal not only for single-phase flow, as reported in the literature, but also for boiling two-phase flow. For low mass fluxes, vanes are not needed, and for very high mass flux the effect of vane angles is negligible.

References

Bhattacharjee, S., Ricciardi, G., & Viazzo, S. (2017). Comparative study of the contribution of various PWR spacer grid components to hydrodynamic and wall pressure characteristics. *Nuclear Engineering and Design, 317*, 22-43. doi:10.1016/j.nucengdes.2017.03.011

Byun, S. J., Shin, C. H., Yoon, J., Kim, H., Lee, J., Eoh, J., & Jeong, J. Y. (2018). Experimental study on the heat transfer enhancement in sub-channels of 6 x 6 rod bundle with large scale vortex flow mixing vanes. *Nuclear Engineering and Design, 339*, 105-115. doi:10.1016/j.nucengdes.2018.09.004

Chang, S. K., Kim, S., & Song, C. H. (2014). Turbulent mixing in a rod bundle with vaned spacer grids: OECD/NEA-KAERI CFD benchmark exercise test. *Nuclear Engineering and Design, 279*, 19-36. doi:10.1016/j.nucengdes.2014.05.013

Chang, S. K., Moon, S. K., Baek, W. P., & Choi, Y. D. (2008). Phenomenological investigations on the turbulent flow structures in a rod bundle array with mixing devices. *Nuclear Engineering and Design, 238*(3), 600-609. doi:10.1016/j.nucengdes.2007.02.037

Cheng, S. H., Chen, H. D., & Zhang, X. Y. (2017). CFD analysis of flow field in a 5 x 5 rod bundle with multi-grid. *Annals of Nuclear Energy, 99*, 464-470. doi:10.1016/j.anucene.2016.09.053

Colombo, M., & Fairweather, M. (2016). Accuracy of Eulerian-Eulerian, two-fluid CFD boiling models of subcooled boiling flows. *International Journal of Heat and Mass Transfer, 103*, 28-44. doi:10.1016/j.ijheatmasstransfer.2016.06.098

Cong, T. L., Zhang, R., Chen, L. J., Zhang, X., & Yu, T. (2018). Studies on the subcooled boiling in a fuel assembly with 5 by 5 rods using an improved wall boiling model. *Annals of Nuclear Energy, 114*, 413-426. doi:10.1016/j.anucene.2017.12.058

Cui, X. Z., & Kim, K. Y. (2003). Three-dimensional analysis of turbulent heat transfer and flow through mixing vane in a subchannel of nuclear reactor. *Journal of Nuclear Science and Technology, 40*(10), 719-724. doi:10.3327/jnst.40.719

Decrecy, F. (1994). The Effect of Grid Assembly Mixing Vanes on Critical Heat-Flux Values and Azimuthal Location in Fuel Assemblies. *Nuclear Engineering and Design, 149*(1-3), 233-241. doi:10.1016/0029-5493(94)90289-5

Feldkamp, L. A., Davis, L. C., & Kress, J. W. (1984). Practical cone-beam algorithm. *Journal of the Optical Society of America a-Optics Image Science and Vision, 1*(6), 612-619. doi:10.1364/Josaa.1.000612

Han, S. Y., Seo, J. S., Park, M. S., & Choi, Y. D. (2009). Measurements of the flow characteristics of the lateral flow in the 6 x 6 rod bundles with Tandem Arrangement Vanes. *Nuclear Engineering and Design, 239*(12), 2728-2736. doi:10.1016/j.nucengdes.2009.09.026

Holloway, M. V., Beasley, D. E., & Conner, M. E. (2008). Single-phase convective heat transfer in rod bundles. *Nuclear Engineering and Design, 238*(4), 848-858. doi:10.1016/j.nucengdes.2007.08.003

In, W. K. (2001). Numerical study of coolant mixing caused by the flow deflectors in a nuclear fuel bundle. *Nuclear Technology, 134*(2), 187-195. doi:10.13182/Nt01-1

In, W. K., Shin, C. H., & Lee, C. Y. (2015). Convective heat transfer experiment of rod bundle flow with twist-vane spacer grid. *Nuclear Engineering and Design, 295*, 173-181. doi:10.1016/j.nucengdes.2015.10.004

Kim, K. Y., & Seo, J. W. (2005). Numerical optimization for the design of a spacer grid with mixing vanes in a pressurized water reactor fuel assembly. *Nuclear Technology, 149*(1), 62-70. doi:10.13182/Nt05-A3579

Li, Z. Z., Chen, D. Q., Wu, D., Xin, S. F., & Li, X. (2021). Subchannel analysis of thermal-hydraulic performance in rod bundle with spacer grid considering anisotropic turbulent mixing. *International Journal of Thermal Sciences, 167*. doi:10.1016/j.ijthermalsci.2021.107039

Mimouni, S., Lavieville, J., Seiler, N., & Ruyer, P. (2011). Combined evaluation of second order turbulence model and polydispersion model for two-phase boiling flow and application to fuel assembly analysis. *Nuclear Engineering and Design, 241*(11), 4523-4536. doi:10.1016/j.nucengdes.2010.12.028

Moon, S. K., Kim, J., Cho, S., Kim, B. J., Park, J. K., Youn, Y. J., & Song, C. H. (2014). Single-phase convective heat transfer enhancement by spacer grids in a rod bundle. *Journal of Nuclear Science and Technology, 51*(4), 543-557. doi:10.1080/00223131.2014.881726

Pickman, D. O. (1972). Design of Fuel-Elements. *Nuclear Engineering and Design, 21*(2), 303-+. doi:10.1016/0029-5493(72)90079-9

Ren, Q. Y., Pan, L. M., Zhou, W. X., Du, S. J., & Li, Z. C. (2018). Phase distribution characteristics of bubbly flow in 5 x 5 vertical rod bundles with mixing vane spacer grids. *Experimental Thermal and Fluid Science, 96*, 451-459. doi:10.1016/j.expthermflusci.2018.04.002

Shen, Y. F., Cao, Z. D., & Lu, Q. G. (1991). An investigation of cross-flow mixing effect caused by grid spacer with mixing blades in a rod bundle. *Nuclear Engineering and Design, 125*(2), 111-119.

Shin, B. S., & Chang, S. H. (2005). Experimental study on the effect of angles and positions of mixing vanes on CHF in a 2x2 rod bundle with working fluid R-134a. *Nuclear Engineering and Design, 235*(16), 1749-1759. doi:10.1016/j.nucengdes.2005.02.006

Takenaka, N., Asano, H., Fujii, T., Wada, T., Matsubayashi, M., & Tsuruno, A. (1996). Three-dimensional void fraction measurement of two-phase flow in a rod bundle by neutron

radiography. *Nuclear Instruments & Methods in Physics Research Section a-Accelerators Spectrometers Detectors and Associated Equipment, 377*(1), 115-118. doi:10.1016/0168-9002(96)00127-1

Tas-Koehler, S., Lecrivain, G., Krepper, E., Unger, S., & Hampel, U. (2020). Numerical investigation on the effect of transversal fluid field deformation on heat transfer in a rod bundle with mixing vanes. *Nuclear Engineering and Design, 361*. doi:10.1016/j.nucengdes.2020.110575

Taş, S., Boden, S., Franz, R., Liao, Y., & Hampel, U. (2023). An experimental study of boiling two-phase flow in a vertical rod bundle with a spacer grid. Part 1: Effects of mass flux and heat flux. *Experimental Thermal and Fluid Science*. doi:10.1016/j.expthermflusci.2023.110903

Tiftikçi, A., Ayhan, H., Kocar, C., & Sökmen, C. N. (2013). *Simulation of spacer grid with mixing vane on a typical pwr fuel rod bundle system using lattice boltzmann method.* Paper presented at the 15th International Topical Meeting on Nuclear Reactor Thermal-Hydraulics, NURETH-15, Pisa, Italy.

Wang, Y., Ferng, Y. M., & Sun, L. X. (2019). CFD assist in design of spacer-grid with mixing-vane for a rod bundle. *Applied Thermal Engineering, 149*, 565-577. doi:10.1016/j.applthermaleng.2018.12.090

Wang, Y. J., Wang, M. J., Ju, H. R., Zhao, M. F., Zhang, D. L., Tian, W. X., . . . Su, G. H. (2020). CFD simulation of flow and heat transfer characteristics in a 5x5 fuel rod bundles with spacer grids of advanced PWR. *Nuclear Engineering and Technology, 52*(7), 1386-1395. doi:10.1016/j.net.2019.12.012

Wei, H. Y., Quintanilla, V., Chen, Y. T., Qi, P. Y., Li, X., Qiao, S. X., & Tan, S. C. (2021). The numerical simulation and analysis of turbulent flow behavior in 5 x 5 fuel rod bundle with split-type mixing vane. *Annals of Nuclear Energy, 159*. doi:10.1016/j.anucene.2021.108324

Wu, J. M., Liang, H. Y., Zhu, F. J., & Lei, J. (2017). CFD analysis of the impact of a novel spacer grid with longitudinal vortex generators on the sub-channel flow and heat transfer of a rod bundle. *Nuclear Engineering and Design, 324*, 78-92. doi:10.1016/j.nucengdes.2017.08.029

Yang, P., Zhang, T., Hu, L. L., Liu, L., & Liu, Y. W. (2021). Numerical investigation of the effect of mixing vanes on subcooled boiling in a 3 x 3 rod bundle channel with spacer grid. *Energy, 236*. doi:10.1016/j.energy.2021.121454